Geochemistry, Geophysics, Geosystems

RESEARCH ARTICLE
10.1029/2019GC008658

Seismic Anisotropy in the Java-Banda and Philippine Subduction Zones and its Implications for the Mantle Flow System Beneath the Sunda Plate

Lingling Wang[1] and Xiaobo He[2]

[1]Department of Marine Sciences, Zhejiang University, Zhoushan, China, [2]Marine Acoustics and Remote Sensing Laboratory,Zhejiang Ocean University, Zhoushan, China

Key Points:
- Systematic investigations of seismic anisotropy in Java-Banda, and Philippines were conducted by source-side *sS* splitting analyses
- Two-dimensional corner flow, squeezed lateral flow by highly arcuate slab, and deflected flow by edge effect are observed
- Dynamic interactions within two adjacent subduction zones are suggested

Supporting Information:
- Supporting Information S1

Correspondence to:
X. He,
xb_he@126.com; xbhe@zju.edu.cn

Citation:
Wang, L., & He, X. (2020). Seismic Anisotropy in the Java-Banda and Philippine Subduction Zones and its Implications for the Mantle Flow System Beneath the Sunda Plate. *Geochemistry, Geophysics, Geosystems*, *21*, e2019GC008658. https://doi.org/10.1029/2019GC008658

Received 27 AUG 2019
Accepted 25 MAR 2020
Accepted article online 27 MAR 2020

Abstract The Sunda Plate is a minor tectonic plate bounded by tectonically active convergent boundaries, below which are subducting: the Philippine Sea Plate to the east and the Indo-Australian Plate to the south and west. It is thus an ideal tectonic setting for investigating the interaction between subduction and asthenospheric flow. To better understand mantle interactions within the two nearly perpendicular subduction zones, we characterize seismic anisotropy by conducting a source-side *sS* splitting analysis, which allows us to improve spatial resolution of anisotropic fabrics, in particular underneath the backarc regions, which are poorly constrained by previous studies. In the backarc of the Java-Banda subduction zone, a gradual fast-axis rotation from trench normal in the west to trench parallel in the east is clearly observed. We attribute this rotation to the interactions between the 2-D corner flow in the Java wedge and a squeezed asthenospheric flow by the highly arcuate Banda slab. In the backarc of the Philippine subduction zone, the fast-axis direction transitions from trench normal in the central south to trench oblique in the north; the trench normal is attributed to the mantle wedge corner flow, whereas the trench oblique is likely deflected by the eastward subduction of the South China Sea Plate. Hence, the mantle flow system beneath the Sunda Plate is composed of various types of flow developed in the mantle wedges. Their interactions play an important role in influencing greatly the regional geodynamics in the upper mantle above the 670-km discontinuity.

Plain Language Summary In this study, we constrained the seismic anisotropy patterns (i.e., the variation of seismic velocities with propagating directions) in the upper mantle beneath the backarc regions of Java-Banda and Philippines located in Southeast Asia by analyzing the fast polarization directions of *sS* wave. It is generally believed that the mantle seismic anisotropy is mainly caused by the crystallographic preferred orientation of mantle minerals such as olivine as the consequence of ductile deformation induced by mantle flow. Therefore, measurements of seismic anisotropy are probably the best tool available to directly probe the mantle flow patterns in the currently tectonic active regions, especially with the importance in understanding dynamic processes such as transport of melt and volatile in the mantle wedge above the subduction zone. Our results depicted that 2-D corner flow, which stands for the mass circulation in the wedge-shaped mantle and is mechanically dragged by the viscously coupled descending slab beneath, is the dominant flow pattern in three studied subduction settings. More importantly, we noted that the 2-D corner flow interacts with the lateral flow, which is orthogonal to the corner flow direction and induced by the highly arcuate Banda slab, and that the flow in north Philippines appears to be deflected by the eastward subducting South China Sea Plate. Our observations reveal the complex dynamic interactions of various types of flow in these tectonic regions.

1. Introduction

The Sunda Plate is a minor tectonic plate located in Southeast Asia; it hosts one of the most complex tectonic units on the planet (Figure 1a). Specifically, it is surrounded by active subducting plate, which includes the Indian-Burma Plate from the west, the Australian Plate from the south, and the opposite subduction of the South China Sea and the Philippine Sea plates beneath the Philippine islands (Bird, 2003). Moreover, it is bounded to the north by the Eurasian Plate. The eastern, southern, and western boundaries of the Sunda

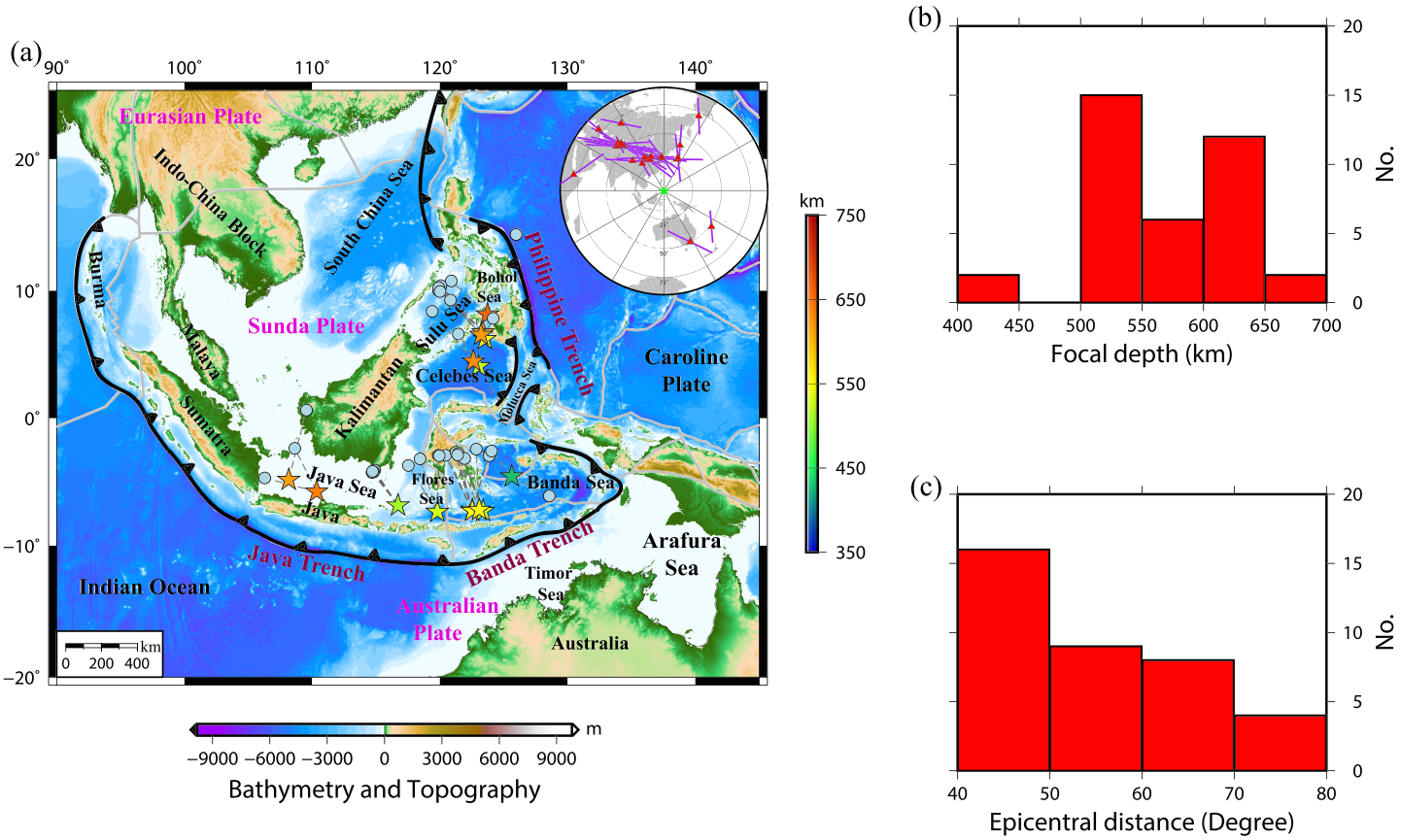

Figure 1. (a) Map showing events (colored stars) and *sS* surface bounce points (light blue circles) used in this study. The color scale for the focal depths is shown in the right, whereas the scale for the bathymetry and topography is shown at the bottom. Dashed lines denote great circle paths for the event *sS* bounce point pairs. The stations (red triangles) with their fast directions (purple bars) used in this study are presented in the top right inset map centered at our study area. (b) Histogram of the focal depths of the events used in this study. (c) Histogram of the epicentral distances calculated for the event-station pairs used in this study.

Plate are tectonically complex and seismically active, whereas the northern boundary is relatively quiescent (Zahirovic et al., 2014).

An intriguing tectonic signature of the Sunda Plate is the Banda arc, which is famous for its 180° curvature (Figure 1a). The extreme curvature of the volcanic chain and the atypical shape of the deformed slab have been attributed to the interactions between the overriding plates, the subducting slab, and the surrounding mantle. The Banda arc thus represents an outstanding example of large-scale deformation of the Earth's lithosphere in response to coupling between the crust, slab, and surrounding mantle (Spakman & Hall, 2010). However, it is still enigmatic how the highly arcuate Banda slab affects the flow both above and below the downgoing slab. In addition, the Sunda Plate is also characterized with the existence of divergent double subduction, which is a form of plate subduction featuring subduction on both sides of one single oceanic plate. More specifically, the Molucca Sea subduction in Southeast Asia has been considered as a Cenozoic example of divergent double subduction, which could thus have played an important role in tectonic evolution of Southeast Asia (Király et al., 2018; Zhang et al., 2017). It is worth mentioning that double-slab subduction with inward-dipping directions is also a characteristic feature of Southeast Asia; for example, the South China Sea Plate is subducting underneath the Philippine Sea Plate, whereas the Philippine Sea Plate is penetrating below the southern Sunda Plate (Figure 1a). Hence, it is an ideal tectonic setting to investigate the interaction how multiple subducting slabs impact their mutual dynamical evolution. However, current understanding of the interactions primarily benefits from numerical simulations (e.g., Király et al., 2016; Lyu et al., 2019), whereas seismic investigations are still limited due to a dearth of seismic data in this region.

The Philippine subduction zone is one of the most complex tectonic settings in the world (Figure 1). In the northern end, the South China Sea Plate is subducting eastward; in the southern end, it is surrounded by the

Sangihe subduction zone where the Molucca Sea Plate is subducting westward; to the central west, the Sulu Sea Plate is subducting eastward. Hence, it is an ideal natural laboratory to study the slab-slab interactions.

Seismic anisotropy—the directional and polarizational dependence of the speed of seismic waves—is a consequence of strain-induced lattice-preferred orientation (LPO) of minerals such as olivine in the upper mantle (Christensen, 1984; Zhang & Karato, 1995). The LPO can be developed by simple shear due to flow gradients existing in the upper mantle, resulting in a fast direction that aligns parallel to the flow direction. Its characterization is thus of importance for understanding the current pattern of asthenospheric flow (e.g., Long & Wirth, 2013). Note that lithospheric compression leads to anisotropy with a fast direction parallel to the strike of mountain belts (e.g., Makeyeva et al., 1992). The most efficient way to characterize the anisotropy in the mantle is through shear wave splitting analysis; shear wave splits into two waves, which travel with different speeds when propagating through an anisotropic zone. Under simple shear, the faster *S* wave polarization direction is often paralleled to the mantle flow direction. Shear wave splitting analysis such as of teleseismic *SKS* splitting has greatly improved our understanding of mantle anisotropy under continents (e.g., Fouch & Rondenay, 2006; Silver, 1996), whereas beneath oceans, our understanding is partial due to limited stations on islands or very sparse deployments of ocean-bottom seismometers (e.g., Bodmer et al., 2015; Lin et al., 2016; Wolfe & Solomon, 1998). Other approaches have been applied to characterize the upper mantle anisotropy under oceans; for example, seismic refraction studies of *Pn* reveal azimuthal anisotropy existing just beneath the Moho (e.g., Shearer & Orcutt, 1986). However, these leave the asthenospheric flow undetected. *SS* wave splitting has been used to constrain anisotropic behaviors beneath *SS* bounce points in the upper mantle (Wolfe & Silver, 1998), but *SS* waveforms appear to be disturbed by crustal reverberations beneath *SS* bounce points (He et al., 2008; Rychert & Shearer, 2010). Phase pairs like *S-SS*, *S-sS*, *ScS-sScS*, and *ScS-ScSScS* have been used to isolate the upper mantle anisotropy beneath surface bounce points by removing the contributions from anisotropy in the upper mantle beneath stations and sources (e.g., Farra & Vinnik, 1994; Fischer & Yang, 1994; Vinnik & Farra, 1992; Yang & Fischer, 1994), but source, bounce point, and receiver splitting should be carefully considered in a proper order (Wolfe & Silver, 1998).

A number of studies of mantle anisotropy have been conducted in Southeast Asia (e.g., Xue et al., 2013), in particular underneath the Sumatra-Java-Banda and Sangihe subduction zones, using local *S*, direct *S*, and *SKS* phases (Di Leo et al., 2012a, 2012b; Hammond et al., 2010). These studies provide information about the regional mantle dynamics of subduction zone. Three-dimensional *P* wave anisotropic tomography results beneath Southeast Asia (Huang et al., 2015) and central Java (Koulakov et al., 2009) and anisotropic Rayleigh wave phase velocity tomography of the Sunda Plate (Legendre et al., 2020) have also offered new clues into the regional mantle dynamics. However, all those studies were subject to poor spatial coverage of seismic stations, in particular beneath the backarc regions, leading to inadequate understanding of mantle wedge dynamics. In addition, in subduction settings, different parts of the subduction system may contribute to the *SKS* splitting, including the overriding plate, the mantle wedge above the slab, the slab itself, and the subslab mantle. Occasionally, the mantle transition zone (e.g., Chang & Ferreira, 2019; Huang et al., 2019), the uppermost mantle (e.g., Ferreira et al., 2019; Wookey et al., 2002), and the lowermost mantle (e.g., He & Long, 2011; Long, 2009; Nowacki et al., 2011) may also contribute, making the interpretation of *SKS* splitting measurements challenging.

We aim to characterize the mantle wedge anisotropy in backarc regions of the Java-Banda and Philippine subduction zones by source-side *sS* splitting analysis, which has been successfully applied to the Izu-Bonin subduction system before (Anglin & Fouch, 2005). This technique first utilizes published *SKS* splitting parameters to remove anisotropic contributions in the station-side upper mantle and then evaluates the corrected *sS* splitting to characterize the upper mantle anisotropy beneath *sS* surface bounce points. Our observations present new constraints on the mantle wedge anisotropy with significantly improved coverage of the two backarc regions. In addition, a global surface wave anisotropic tomography model by Debayle et al. (2016) and a regional *Vp* velocity model UU-P07 by Hall and Spakman (2015) are also incorporated to discuss the regional mantle dynamics.

2. Data, Methods, and Analyses

Data in our study come from 30 global broadband stations (Figure 1a). We selected earthquakes that occurred at depths greater than 400 km and used a magnitude threshold of Mw = 5.8 for all events; the reason why

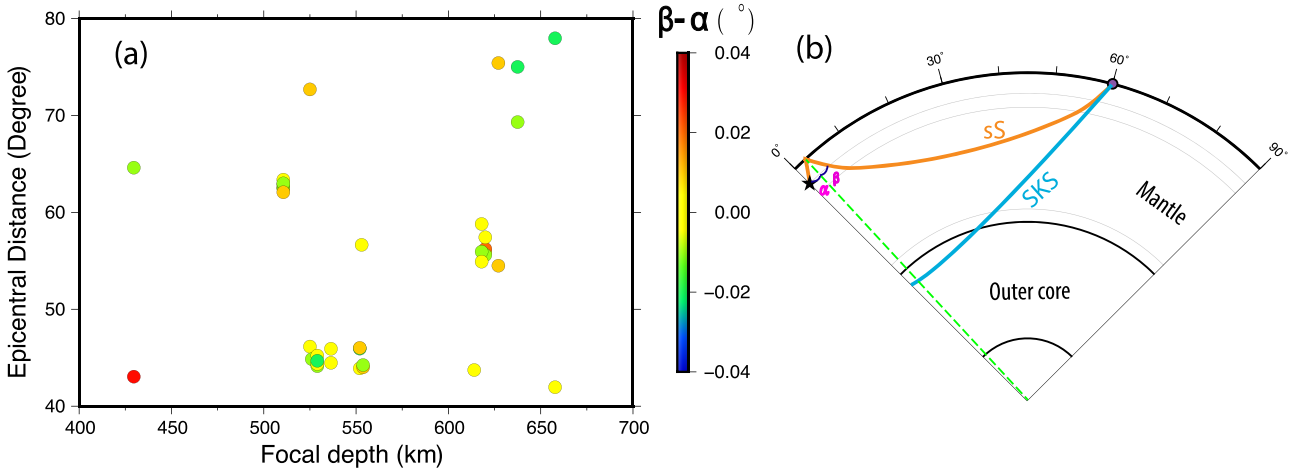

Figure 2. (a) The colored circles denote the difference between the incident angle (α) and the take-off angle (β) of the *sS* wave beneath its bounce point for all focal depth-epicentral distance pairs used in this study, which is calculated according to the IASP91 model (Kennett & Engdahl, 1991) using the TauP Toolkit (Crotwell et al., 1999). The color scale for the angle difference is shown in the right. (b) Schematic raypath geometry of the source-side *sS* splitting technique. If seismic anisotropy in the upper mantle beneath the receiver (solid circle) can be well constrained by *SKS* splitting analysis and the lower mantle is isotropic, then any splitting of *sS* wave as shown is attributable to seismic anisotropy in the upper mantle beneath its bounce point.

we restricted our analysis to deep events will be discussed further in the part of method descriptions. We obtained 37 teleseismic *sS* measurements from 15 events ranging in hypocentral depth from 430 to 658 km (Figure 1b) recorded at 30 stations with epicentral distances ranging from 40° to 80° (Figure 1c). Information for all events used in this study is given in Table S1 in the supporting information. Anisotropic parameters of 30 stations used for removing the anisotropic contributions beneath the stations are compiled from a range of previous publications (Barruol & Ben Ismail, 2001; Barruol & Hoffman, 1999; Chang et al., 2011, 2015; Cherie et al., 2016; Fouch & Fischer, 1996; Hanna & Long, 2012; Helffrich et al., 1994; Huang et al., 2011; Király et al., 2012; Liu et al., 2008; Makeyeva et al., 1992; Vinnik et al., 1992; Wolfe & Vernon III, 1998). A full list is provided in Table S2.

Instead of measuring seismic anisotropy beneath seismic stations, here we aim to characterize seismic anisotropy in the upper mantle beneath *sS* surface bounce points by employing the source-side *sS* splitting technique. Such a technique has been successfully applied in Izu-Bonin subduction zone (Anglin & Fouch, 2005). The main procedure of this technique is to first correct for station-side upper mantle anisotropy and then characterize the anisotropy in the upper mantle beneath *sS* surface bounce points. The last step is to project the fast directions measured at the station back to the true orientation beneath the corresponding *sS* bounce point, because the splitting measured at the station is from upgoing rays, whereas the anisotropy beneath the *sS* bounce point is sensed by downgoing rays (Anglin & Fouch, 2005).

Here we assume that splitting parameters for upgoing and downgoing paths for *sS* phases are the same, which is true when the olivine *a*-axis is horizontal and anisotropy does not vary significantly in the region beneath the bounce point and also because the upgoing and downgoing paths are nearly symmetric (the different between the incident angle [α] and the take-off angle [β] is very small; Figure 2a). According to the assumption, we thus conclude that (i) the constrained fast directions after being projected back to the bounce-point side can be directly taken as the fast directions in the upper mantle beneath the *sS* bounce points and (ii) the delay times for the upgoing paths are equal to those for the downgoing paths, suggesting that the delay time in the upper mantle beneath the bounce point can be approximately considered as half of the measurement from *sS* splitting after corrected the station-side contribution. This approximation is also reasonable because the analysis is restricted to *sS* phases from deep earthquakes (depth of >430 km in this study), and the contributions from the structures below the source can accordingly be negligible (isotropic or weak anisotropy).

In order to characterize the anisotropy near the source side, careful station selection is very important to avoid potential errors from the station side. For this reason, the analysis is limited to stations only with simple splitting pattern in the upper mantle (i.e., no strong variations with back azimuths). Those stations with complex anisotropy are all excluded (Walpole et al., 2017). The parameters along with the corresponding

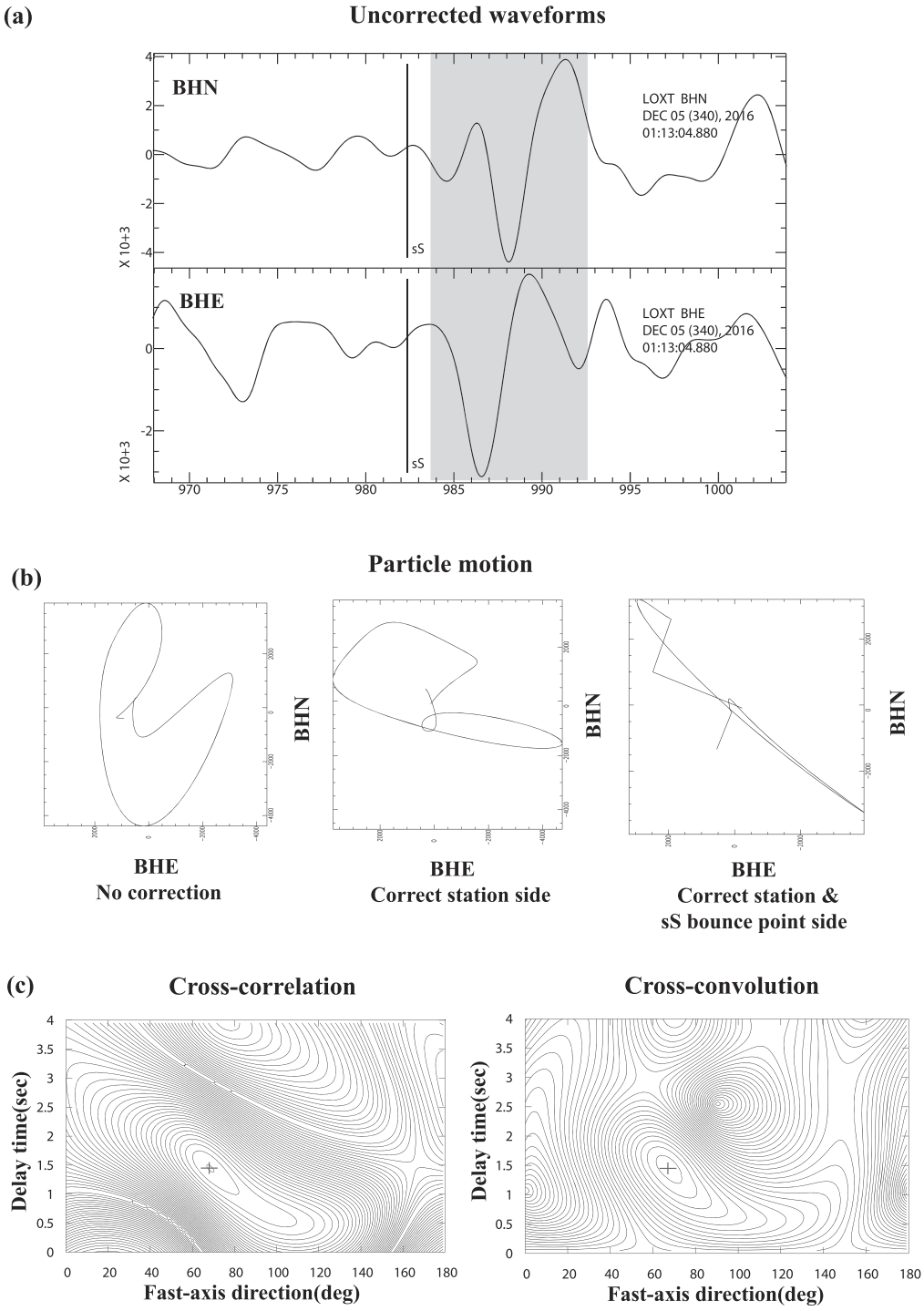

Figure 3. An example of the source-side *sS* splitting measurements, measured for the event on 5 December 2016 recorded at the station LOXT. (a) Uncorrected horizontal component waveforms. The shaded gray region indicates the time window used in the splitting analysis. (b) The diagnostic plots for the particle motions obtained by cross-correlation method: from left, uncorrected particle motion, corrected receiver side, corrected receiver, and source sides. (c) The map of error surface for the cross correlation (left) and the cross convolution (right) (Menke & Levin, 2003). The splitting parameters obtained (at the station) using both methods are well constrained and are in good agreement with each other.

references are all listed in Table S2. In addition, we consider *sS* phases recorded in the epicentral distances ranging from 40° to 80°, which ensures the difference in incident angle between *SKS* and *sS* at the station to be small enough that the correction for the upper mantle contribution of station side will be appropriate; the errors in correction due to the difference in incident angle are generally less than the uncertainty in the source-side splitting technique (Nowacki et al., 2012).

All records were visually inspected to ensure good waveform quality and high signal-to-noise ratios. For the *sS* phases, we applied a two-pass, two-pole Butterworth bandpass filter with corner frequencies at 0.05 and 0.5 Hz—which represent the typical frequency band for teleseismic signals (He & Long, 2011)—to the data. We visually selected arrivals by calculating the theoretical arrival times according to the IASP91 model (Kennett & Engdahl, 1991) and manually chose a time window for the *sS* splitting, which encompasses one full period of the wave and was optimized to identify the best-constrained splitting parameters.

After correcting the station-side's contribution, the cross-correlation (Bowman & Ando, 1987) and the cross-convolution (Menke & Levin, 2003) methods are used together to constrain the splitting parameters (ϕ and δt). We computed 95% confidence regions and rejected measurements when those derived from two methods are not in agreement within 15° and 0.5 s for ϕ and δt, respectively. We used those derived from the cross-correlation method as the final splitting parameters. In addition, we applied a strict set of criteria to select the optimum splitting results: (i) All horizontal component waveforms are visually inspected to ensure good waveform quality and high signal-to-noise ratios; (ii) clear elliptical particle motion before correction; and (iii) clear linearization of particle motion after corrected. An example of the *sS* splitting measurement, measured for the event occurred on 5 December 2016 and recorded by the station LOXT, is shown in Figure 3. For this measurement, both the cross-correlation and cross-convolution methods yield well-constrained estimates of the splitting parameters ($\phi = 68°$ and $\delta t = 1.45$ s), which are measured at the station. Finally, our analysis yields a total of 37 *sS* splitting measurements, in which 24 data sample the Java-Banda subduction zones and 13 data are located in the Philippine subduction zone.

3. Results

The resulting spatial distributions of 37 individual measurements are shown in Figure 4. Details of individual well-defined splitting parameters at *sS* bounce points can be found in Table S3. The resulting fast orientations in the Java wedge are nearly N-S oriented (trench normal), which is subparallel to the absolute plate motion (APM) direction of the Indo-Australian Plate calculated based on the HS3 (Pacific hot spot reference frame) model (Gripp & Gordon, 2002) or the NNR (no-net-rotation frame) model (DeMets et al., 1994). By contrast, a gradual rotation of resulting fast orientations from trench normal in the west to trench parallel (more precisely, parallel to the curvature of the Banda arc) in the east is clearly observed in the neighboring Banda wedge. In the Philippine wedge, the resulting fast orientations remain scattered; W-E (trench normal, parallel to the APM direction of the Philippine Sea Plate) is dominant, but trench-oblique orientations are also seen in the north.

The sample average (μ) with the standard deviation (σ) of the 37 δt is 0.96 ± 0.36 s, in which 0.90 ± 0.33 s occurs to the Java-Banda wedge, whereas 1.00 ± 0.44 s occurs to the Philippine wedge. The summary of δt is presented in Figure S1. The resulting average δt is slightly smaller than the average value (1.25 s) from oceanic islands calculated by Király et al. (2012) from the Global Splitting Database (http://www.gm.univ-montp2.fr/splitting/) (Wustefeld et al., 2008) but which is in reasonable agreement with previous local studies, for example, 0.90 ± 0.14 s in the southernmost Indochina Peninsula (Yu et al., 2018), ~1 s in the Sumatra wedge (specifically, measurements are made for the stations located above the 150-km slab contour) (Hammond et al., 2010), and 0.34–1.08 s in the Banda wedge measured from local *S* splitting (Di Leo et al., 2012a). The larger δt (of 1.6–2.4 s in Sumatra, Collings et al., 2013; ~1.6 s in Java, Hammond et al., 2010; and 1.13–1.38 s in Banda, Di Leo et al., 2012a) has been primarily attributed to subslab mantle flow, rather than the flow in the mantle wedge, and the larger δt all comes from *SKS* splitting measurements.

We emphasize here that our data set (34 out of 37 event-station pairs) largely exhibits that each event has been recorded by multiple stations (one-to-many type); only remaining three event-station pairs belong to one-to-one type. The one-to-many type of pairs allows us to examine the consistency of measurements. Because the same event was recorded by multiple stations with different anisotropic parameters, it can reflect the good reliability of our measurements if the constrained parameters are in reasonable agreement between each other. In addition, 14 pairs (14 out of 37) show that multiple events were recorded by

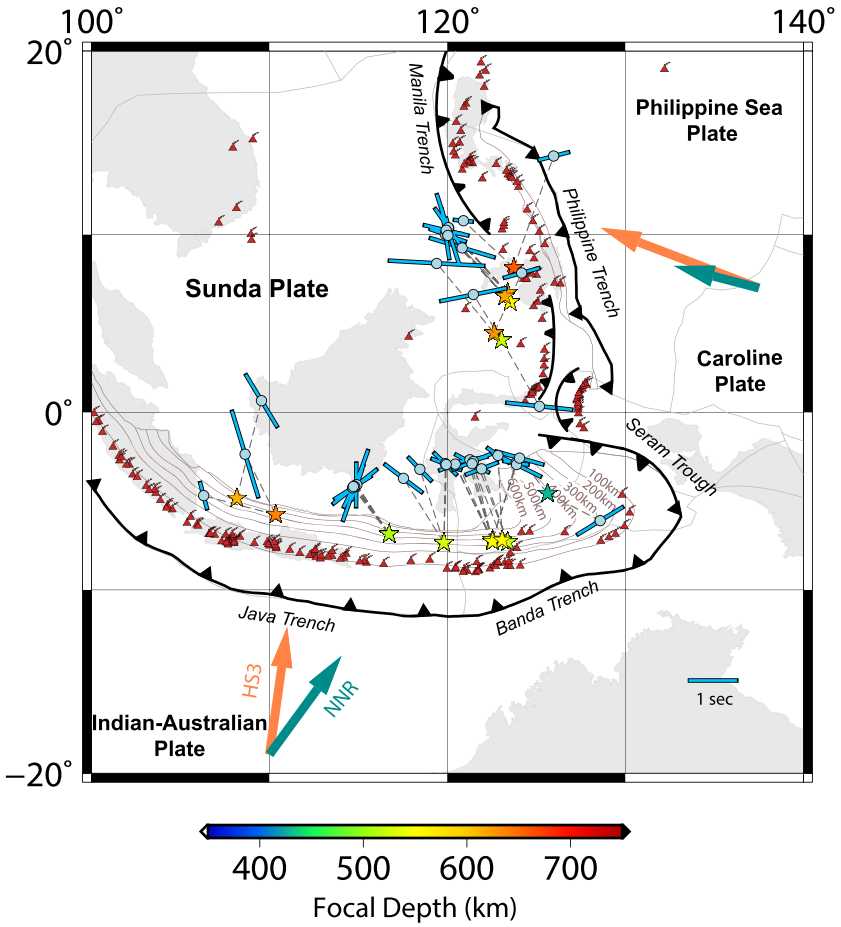

Figure 4. All splitting results in this study are plotted at *sS* surface bounce points (light blue circles). Bars are oriented in the fast direction, and their lengths are proportional to the delay times. Colored stars are seismic events. The color scale for the focal depths is shown at the bottom. Solid red triangles denote Quaternary volcanoes. The black sawtooth lines show major plate boundaries. The contour lines show depths to the upper boundaries of the subducting slabs with an interval of 100 km from Slab2 (Hayes et al., 2018). Arrows indicate plate motion according to absolute plate motion (APM) models (HS3: Pacific hot spot reference frame, Gripp & Gordon, 2002, denoted with sienna arrows; NNR: no-net-rotation frame, DeMets et al., 1994, denoted with light sea green arrows).

one station (many-to-one type), which offers another way to examine the consistency of measurements. For this purpose, we plot the 34 measurements of one-to-many type (Figure S2) and 14 measurements of many-to-one type (Figure S3) to examine its consistency, and the quantitative comparisons are summarized in Figures S2b and S2c. This strongly supports the reliability of our measurements. In addition, these tests show that in general, no significant variations in observed splitting are observed as a function of event-to-station azimuth (although the azimuth range is limited), which indicates relatively simple anisotropic structure beneath many *sS* surface bounce points.

Determining the primary source of anisotropy that contributes to *sS* splitting can be difficult, because the observed splitting is an integrated result along the raypath defined by the source and receiver. Hence, any part of the anisotropic layers in the Earth's interior, which *sS* has traveled through, can be possible source for the observations. If we assume that the contribution from the station-side upper mantle has been fully accounted and corrected by *SKS* splitting, then remaining source regions are all residing in the upper mantle beneath the *sS* bounce point, including the overlying lithosphere, the mantle wedge, and the slab itself. We can readily exclude the subslab mantle as a contributor, thanks to the source-receiver geometry.

4. Seismic Anisotropy in Subduction Zones

4.1. Mechanisms and Sources of Seismic Anisotropy

The primary cause of seismic anisotropy in the upper mantle is the LPO of olivine (e.g., Zhang & Karato, 1995), which can develop in the upper mantle due to shearing induced by mantle flowing

(e.g., Wolfe & Silver, 1998). In a subduction zone environment, where the mantle wedge may be hydrated by water released from downgoing slab, B-type olivine LPO may develop. In B-type olivine fabric, which develops under water-rich conditions, the [0 0 1] direction is parallel to the flow direction, and the (0 1 0) plane is parallel to the flow plane, which have been invoked to explain trench-parallel anisotropy. More specifically, in a flow field, the crystallographic fast axis of B-type olivine is oriented perpendicular to flow. Therefore, fast-axis values would be rotated 90° from other types of olivine (e.g., Jung & Karato, 2001; Karato et al., 2008; Katayama & Karato, 2006), but B-type olivine is dominant in the forearc, whereas A-type olivone—the well-known fabric developed under water-poor conditions, in which the [1 0 0] axis is subparallel to the shear direction and the (0 1 0) plane is subparallel to the shear plane—is still pervasive in the backarc (Karato et al., 2008; Zhang & Karato, 1995). Hence, we consider A-type olivine LPO fabrics in the asthenosphere as the leading candidate to explain our observations. In the following parts, we will explain why we rule out other anisotropic contributions from the slab itself, the overriding plate, the subslab mantle, and the mantle below the source.

The *sS* bounce points are abundantly located underneath seas such as the Java Sea, Banda Sea, and Sulu Sea (Figure 1). The overlying lithosphere is thus known for being thin (its thickness is about 50 km or less given by a *P* wave tomographic result of Huang et al., 2015, and a Rayleigh wave phase velocity image of Legendre et al., 2020). This equates to an approximate delay time of 0.4 s assuming 4% anisotropy and an *S* wave velocity of 4.6 km/s (e.g., Eakin et al., 2010). In reality, the resulting δt could be much less than 0.4 s because 0.1–0.3% anisotropy is imaged in the overlying lithosphere by the *P* wave and Rayleigh wave azimuthal anisotropy tomography (Huang et al., 2015; Legendre et al., 2020). It therefore seems unlikely that the constrained δt of 0.96 ± 0.36 s in this study is generated primarily from the overlying lithosphere, although we cannot rule out its contribution.

Another possible source of anisotropy comes from the slab itself. Oceanic lithosphere develops frozen-in anisotropy as it matures (e.g., Debayle & Ricard, 2013), and its magnitude seems to positively correlate with the spreading rate in the mid-ocean ridge (e.g., Gaherty et al., 2004; Song & Kim, 2011). It has been suggested that oceanic lithosphere can retain the frozen-in anisotropy through subduction (e.g., Audet, 2013; Chen et al., 2015) but slab anisotropic magnitude varies from region to region; for example, Chen et al. (2015) suggested the contribution to shear wave splitting from the downgoing Philippine Sea Plate in Taiwan to be 0.13 to 0.45 s, and Huang et al. (2011) estimate the anisotropic magnitude contributed from the subducting Pacific Plate in Japan to be minor (0.10 to 0.32 s). It is noteworthy that, although δt up to 0.45 s has been occasionally detected, the events used to observe such a large δt are all at intermediate depths. At these depths, hydrated faults—likely developed in the trenches due to slab bending—have played an important role in producing the observed slab anisotropy (e.g., Abers, 2000; Faccenda et al., 2008). However, the events used in this study are all from the depths deeper than 300 km; thus, it is unlikely to produce such a strong anisotropy within a downgoing dry slab. This scenario is supported by an observation of insignificant deep slab anisotropy ($\delta t < 0.15$ s) in Tonga (Kaneshima, 2014). Moreover, a careful analysis of local *S* and teleseismic *SKS* splitting in the southern Italy subduction system also revealed that the main source of anisotropy in the subduction zone is the asthenosphere and the slab is a weakly anisotropic region (Baccheschi et al., 2011). All these observations seemingly support insignificant anisotropy from the subducting plates, in particular at deep depths.

Strong anisotropy in the subducting Nazca slab has been observed beneath Peru, but it was attributed to overprinted fossil fabric during subduction, instead of the frozen-in anisotropy formed at the mid-ocean ridge. To produce such a strong anisotropy, the deformed slab must therefore be sufficiently weak so that its original fabric can be modified. However, the issue as to whether other subducting slabs behave also similarly to the Nazca slab remains mostly unaddressed. Song and Kim (2011) have observed a 2- to 6-km subcrustal layer with ~7% anisotropy preserved in the subducting Cocos Plate beneath central Mexico. A subsequent receiver function study by Audet (2013) also suggested the presence of strong anisotropy within uppermost mantle of subducting oceanic plates, but the observed anisotropy is characterized with more variable parameters in thickness and anisotropic magnitude in the forearcs of Nankai, Cascadia, Mexico, and Costa Rica subduction zones. It appears that the existence of such a strong anisotropic layer within the downgoing slabs is all limited to shallow subduction zones; the issue as to whether this anisotropic layer also occurs in other subduction zones requires further investigations. Hydrated faults in the subducting oceanic plate have been suggested to explain the trench-parallel fast axes of seismic anisotropy but which are only measured at stations in the forearc (Abers, 2000; Faccenda et al., 2008). Again, there are seemingly no direct

observations to support the existence of strong anisotropy within the downgoing slabs at depths deeper than 300 km. With all the evidence, we therefore conclude that the main source of observed splitting is the mantle wedge asthenosphere and the contribution from the slab or the overriding lithosphere is negligible.

In addition, we also plot the measured δt as a function of focal depth (Figure S4) to examine if there exists a depth-dependent signature. It demonstrates that no notable depth-dependent δt is observed, suggesting that the anisotropic contributions to *sS* splittings are primarily confined in the upper mantle (above 430-km depth), whereas that below 430-km depth is insignificant. Otherwise, we may expect to see a positive correlation between focal depth and δt (i.e., δt increases with deepening of events). It in turn suggests that the constrained parameters can adequately represent the upper mantle anisotropic characteristics beneath the *sS* bounce point. Lack of strong depth-dependent signature does not fully exclude the existence of anisotropy in the lower mantle transition zone (LMTZ) and uppermost lower mantle, which has been suggested to take place in subduction zones (e.g., Chang & Ferreira, 2019; Faccenda, 2014; Faccenda et al., 2019; Ferreira et al., 2019; Huang et al., 2019). The reason for this is because the number of events in the LMTZ used in this study is very limited and also, no events are from the uppermost lower mantle. Another possible reason is that ringwoodite (the dominant mineral in the LMTZ) seemingly has a different slip systems compared to olivine (e.g., Miyagi et al., 2014); increasing the raypath length through the LMTZ may thus not simply enhance the *sS* splitting magnitude. Moreover, flow directions in the upper mantle and transition zone would be different from each other, which may further complicate the interpretations. It is also worth mentioning that a seismological study pointed out that the LMTZ is largely isotropic (e.g., Fouch & Fischer, 1996), which has been corroborated by another mineral physics study by Ohuchi et al. (2014).

4.2. Flow Models in Subduction Systems

In a subduction system, the classical flow model is composed of a simple 2-D corner flow in the mantle wedge (i.e., above the subducting slab), which is induced by viscous coupling between the downgoing slab and the overlying mantle, along with an entrained flow (i.e., beneath the subducting slab) when a strong coupling exists between the downgoing slab and subslab mantle (e.g., Long & Silver, 2008). The anisotropy resulting from the 2-D corner flow or the slab-entrained flow often exhibits trench-normal fast directions (more precisely, parallel to the APM of subducting slabs). However, due to the influences from a number of factors such as trench migration, proximity to slab edges, slab morphology, existence of slab window, local thermal anomaly, and volatile distribution, the resultant flow pattern and anisotropic parameters exhibit a large variations worldwide (see a more detailed review by Long, 2013); specifically, small-scale flow and 3-D toroidal flow have been found in subduction zones (e.g., Faccenna & Becker, 2010; Venereau et al., 2019), and trench-parallel flow also exists below the subducting slabs (e.g., Russo & Silver, 1994). In addition, slab-slab interaction between two neighboring subducting plates (e.g., Király et al., 2018) also likely plays a role in complicating the flow fields in subduction zones. Hence, careful analysis of the observed anisotropic parameters by jointly considering splittings from different types of waves, such as *P* wave, local *S* wave, source-side *S* wave, teleseismic *SKS*, and surface wave, is important to lead to correct interpretations, because they are characterizing with different resolutions in vertical and horizontal directions.

5. Comparisons With Previous Studies

5.1. Comparison With *SKS* Splitting Results

Because no *SKS* splitting analyses have been performed before in the Philippine subduction zone, the comparison here will only focus on the Java-Banda subduction zone (Figure 5). The *SKS* splitting measurements in this region are mainly given by Di Leo et al. (2012a) and Hammond et al. (2010), in which the measurements of Hammond et al. (2010) are abundantly measured at stations in the arcs, whereas the results of Di Leo et al. (2012a) are primarily from the stations in the backarcs or beyond. As we mentioned above, all the *SKS* splittings have been attributed to mantle flow beneath the slabs. As a result, the δt from *SKS* splitting is slightly larger than that of 0.90 ± 0.33 s in the mantle wedge given by this study; specifically, 1.22 ± 0.40 s occurs to the stations in the arcs (Hammond et al., 2010), whereas 1.23 ± 0.48 s is corresponding to the stations in the backarcs (Di Leo et al., 2012a).

Notably, a sharp fast-axis transition from trench normal in Sumatra to trench parallel in Java and Banda is observed in the *SKS* splitting measurements by Hammond et al. (2010), and a similar observation was observed from source-side *S* wave splitting studies (Lynner & Long, 2014; Roy et al., 2017; Walpole et al., 2017). This abrupt change in fast axis may be associated with the variations of slab dipping angle from Sumatra to Java (Srijayanthi & Kumar, 2019). For the measurements of Di Leo et al. (2012a) from the stations

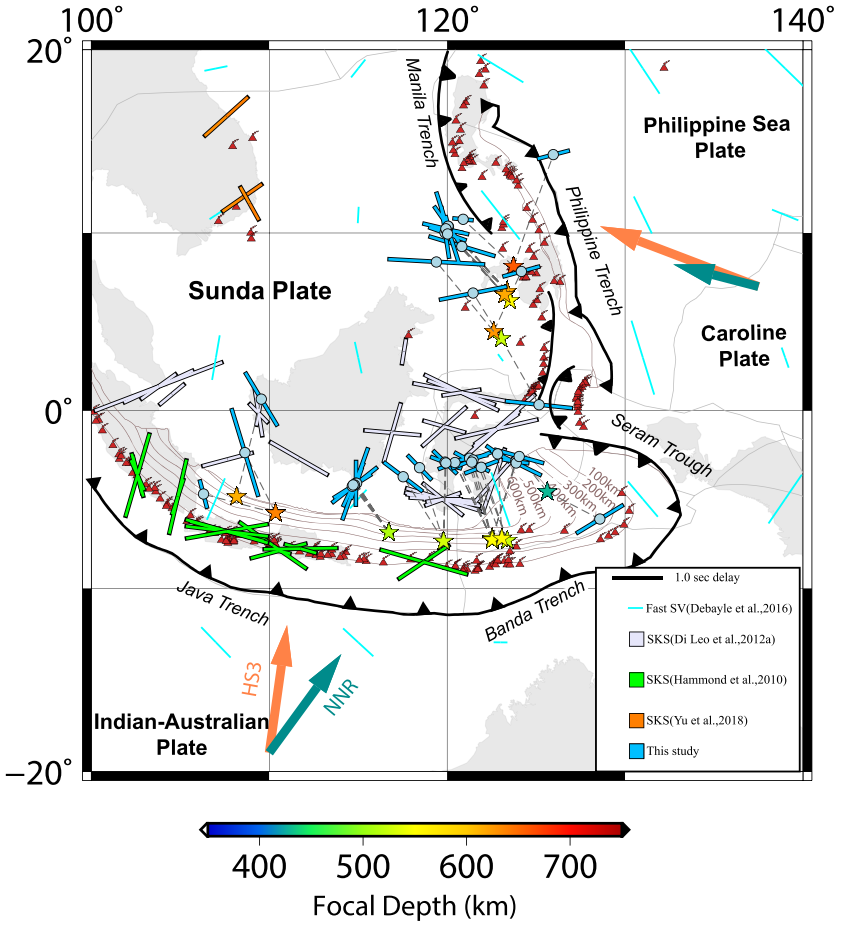

Figure 5. Comparison of *sS* splitting observations in this study (blue bars) and previous *SKS* splitting results. Bars represent orientation of the fast direction, and its color represents different studies (lavender for *SKS* results of Di Leo et al., 2012a; green for *SKS* results of Hammond et al., 2010; orange for *SKS* results of Yu et al., 2018; and cyan for fast SV directions of Debayle et al., 2016, at a depth of 100 km). Their lengths are proportional to delay times, and the length of the cyan bars is proportional to the maximum amplitude of azimuthal anisotropy at this depth. The arrow (sienna and light sea green) convention is similar to that in Figure 4.

away from the arcs, the fast-axis orientations are more variable, but the dominant pattern can still be seen: trench normal in the west (Java) and trench parallel in the east (Banda). Overall, this pattern is in reasonable agreement with that we observed in this study (Figure 5), but our observations show a smoother transition from trench normal in Java to trench parallel in Banda. We will discuss what possible mechanisms can produce such a rotational pattern in fast directions in the following sections.

5.2. Comparison With Local *S* and Source-Side *S* Splitting Results

Local *S* wave splitting measurements are abundant from the stations in the arcs (approximately located above the 100- to 150-km slab contour) (Figure 6). Fast directions are mostly oriented in trench parallel in the Java subduction zone, whereas δt exhibits a large variations in 0.1–1.3 s (92% $\leq$ 0.6 s) (Hammond et al., 2010). In the south Philippine subduction zone (where the Sangihe subduction zone is located in the west), δt varies from approximately 0.34–0.53 s measured at the stations located in the arcs to approximately 0.53–0.65 s measured at the stations located above the deeper slab contour (more than ~380 km), and fast directions change from trench parallel to trench normal (Di Leo et al., 2012b). This trench-normal fast direction pattern is also observed to the north from our measurements. In both subduction zones, trench-parallel fast directions are attributed to aligned, possibly melt-filled cracks beneath the volcanic arcs and fossil anisotropy in the overlying lithosphere (Di Leo et al., 2012a, 2012b; Hammond et al., 2010).

Source-side *S* splitting measurements are primarily performed along the highly arcuate Banda arc (Figure 6); the fast axis displays orientations in line with the curvature of the arc, and δt varies between 0.50 and

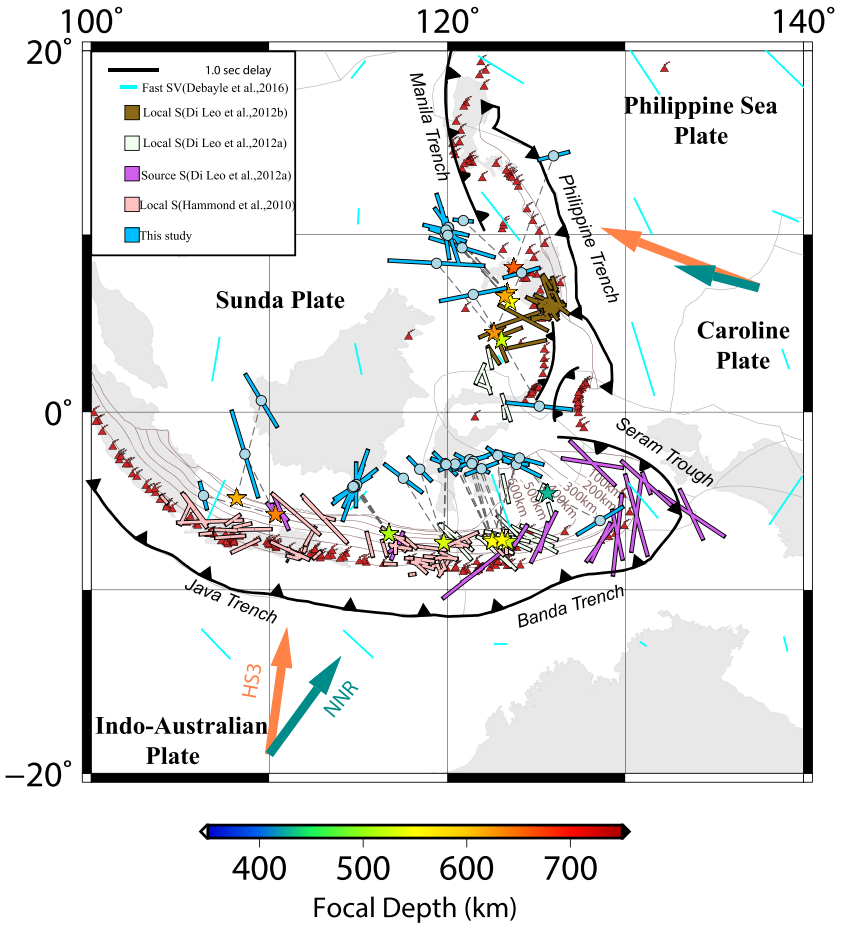

Figure 6. Comparison of *sS* splitting observations in this study (blue bars) and previous local *S* and source-side *S* splitting results. Bars are oriented in the fast direction and colored by different studies (honeydew for local *S* measurements of Di Leo et al., 2012a; goldenrod for local *S* results of Di Leo et al., 2012b; medium orchid for source-side *S* study of Di Leo et al., 2012a; hammond pink for local *S* measurements of Hammond et al., 2010; and cyan for fast SV directions of Debayle et al., 2016, at a depth of 100 km). Their lengths are proportional to delay times. The arrow (sienna and light sea green) convention is similar to that in Figure 4.

1.70 s. This observation is consistent with that from *SKS* splitting measurements (Figure 5); existence of trench-parallel subslab mantle flow was suggested to explain this signature (Di Leo et al., 2012a).

6. Discussion

6.1. Mantle Flow in the Java-Banda Subduction Zone

The most striking tectonic feature in the Java-Banda subduction zone is the Banda arc, which is famous for its 180° curvature; it has been attributed to rollback of the Banda slab (Spakman & Hall, 2010). The Banda arc thus serves as an exceptional example of large-scale deformation of the Earth's crust in response to the coupling between crust, slab, and surrounding mantle (Spakman & Hall, 2010), but how this arcuate Banda slab affects the flow, both above and below the slab, has not been fully understood.

Trench-normal fast directions are clearly seen in our measurements in the Java subduction zone, and the directions gradually become trench oblique to the east (Figure 4). A slab gap within the downgoing Indian Plate has been suggested to exist between Sumatra and Java and induce a 3-D trench-parallel flow in the Sumatra mantle wedge (Huang et al., 2015). However, it appears that the trench-normal orientations observed here have not been affected by this slab gap. In addition, this trench-normal signature is also evident in the surface wave anisotropic tomography results given by Debayle et al. (2016) (Figures 5 and 6). We attribute these trench-normal fast directions to the simple 2-D corner flow in the mantle wedge induced by viscous coupling between the downgoing Indian slab and the overlying mantle.

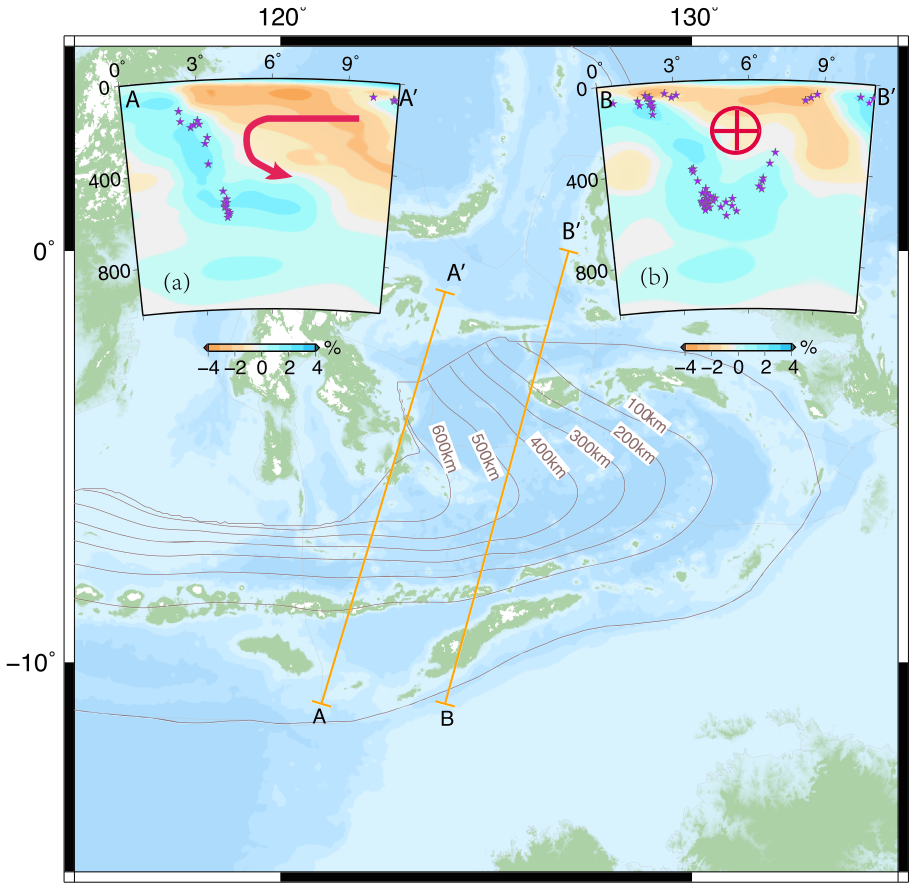

Figure 7. Interpretations of mantle flow with the help of *Vp* velocity model by Hall and Spakman (2015) in the Banda subduction zone. Two vertical profiles along AA′ and BB′ are presented in the inserts (a and b), respectively. Earthquakes ($M > 5$ and spanning from 1990 to 2019, and the catalog is from USGS) are denoted with stars. The bent arrow in the insert (a) denotes the 2-D corner flow in the wedge, and the circle with a cross in the insert (b) represents westward moving flow squeezed by the subduction of the highly arcuate Banda slab. The fast anomalies with seismicity clearly delineate the downgoing slabs; the slow anomalies describe the asthenospheric materials in the mantle wedge.

The most striking observation in this study is that a directional rotation from trench normal to trench parallel is clearly observed from Java to Banda (Figure 4). The trench-parallel (more precisely, in line with the curvature of the Banda arc) fast directions have been attributed to oblique supraslab shear layers in the Banda mantle wedge in Banda (Di Leo et al., 2012a). Here we propose that they are probably developed by a lateral flow due to asthenospheric materials squeezed out of the mantle wedge with limited space caused by the subduction of the highly arcuate Banda slab. This scenario can be approximately treated as squeezing flow by two oppositely dipping and adjacent subducting slabs.

To better understand this process, a previous tomographic model UU-P07 provided by Hall and Spakman (2015) is incorporated to help with interpretations (Figure 7). The fast anomalies with seismicity clearly delineate the downgoing slabs, and slow anomalies possibly reflecting the asthenospheric materials are evident in the mantle wedge; the asthenospheric materials trapped in the mantle wedge can be squeezed as a result of double subduction of two oppositely dipping and adjacent subducting slabs. Figure 7b displays this process as to how the lateral flow can be developed when the subduction of the highly arcuate Banda slab occurs. We further attribute the smooth transition in fast directions from trench normal in Java to trench parallel in Banda as a result of the interactions between the 2-D corner flow in the west and the lateral flow (probably westward moving) in the east. The interpreted 2-D corner flow and deflected lateral flow in this area are both displayed schematically in Figure 8. Our observations thus demonstrate that dynamic interactions between asthenospheric flows are actively taking place in the complex tectonic region. In addition, the subslab mantle flow around the highly arcuate Banda slab as suggested by Di Leo et al. (2012a), if it exists, may also take part in the interactions.

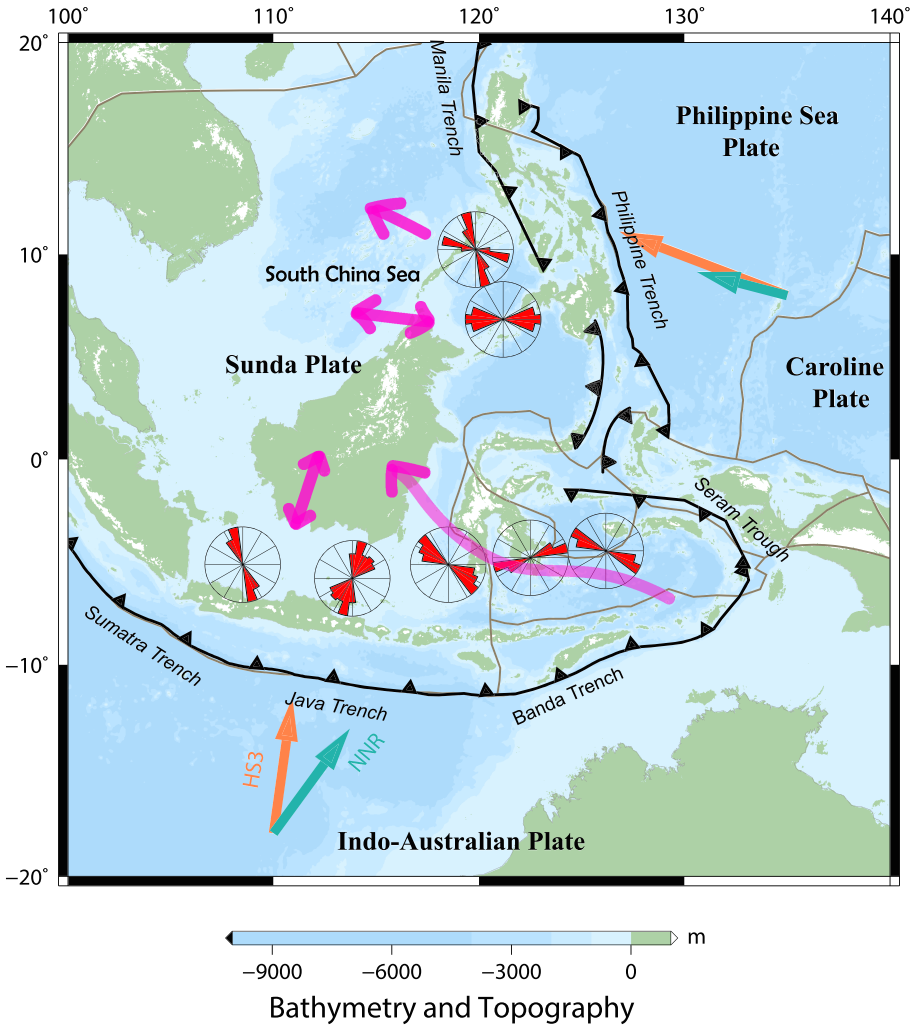

Figure 8. Map showing the rose diagram of fast axis of anisotropy from the source side *sS* splitting for different segments of subduction zones (bin size 15°). The interpreted mantle flows are denoted with pink arrows, in which the curved bar with one arrow denotes the squeezed lateral flow by the highly arcuate Banda slab and the straight bar with one arrow displays the deflected flow due to edge effect of the eastward subduction of the South China Sea Plate, whereas the bars with two arrows denote the 2-D corner flow. The arrow (sienna and light sea green) convention is similar to that in Figure 4.

Although the Banda subduction zone has experienced slab rollback as suggested by Spakman and Hall (2010) and slab rollback additionally facilitates trench-parallel mantle flow below the subducting slabs (e.g., Long & Silver, 2008), interpretations of trench-parallel fast directions need to be treated with caution. The reasons lie in that (i) at shallow depths (<50 km) trench-parallel fast directions are possibly due to trench-parallel faults associated with faulting and hydration by slab bending within the slabs (Faccenda et al., 2008; Walpole et al., 2017), and (ii) at deeper depths (50–250 km) trench-parallel fast directions can be explained by tilted transverse isotropy with a slow symmetry axis pointing normal to the plane of the slab. This scenario can be produced by subducting oceanic asthenosphere with weak azimuthal but strong radial anisotropy in steep subduction settings (Song & Kawakatsu, 2012, 2013) like the Banda subduction zone. Hence, observations of trench-parallel fast directions may not be directly associated with trench-parallel subslab flow (Walpole et al., 2017). As a result, the issue as to whether trench-parallel mantle flow exists beneath the subducting Banda slab may not be conclusive.

6.2. Mantle Flow in the Philippine Subduction Zone

According to our observations, the fast directions change from trench normal in the central Philippine subduction zone to trench oblique to the north, where they are in close proximity to the edge of the eastward subducted South China Sea Plate. The trench-normal signature is consistent with that observed in the local *S*

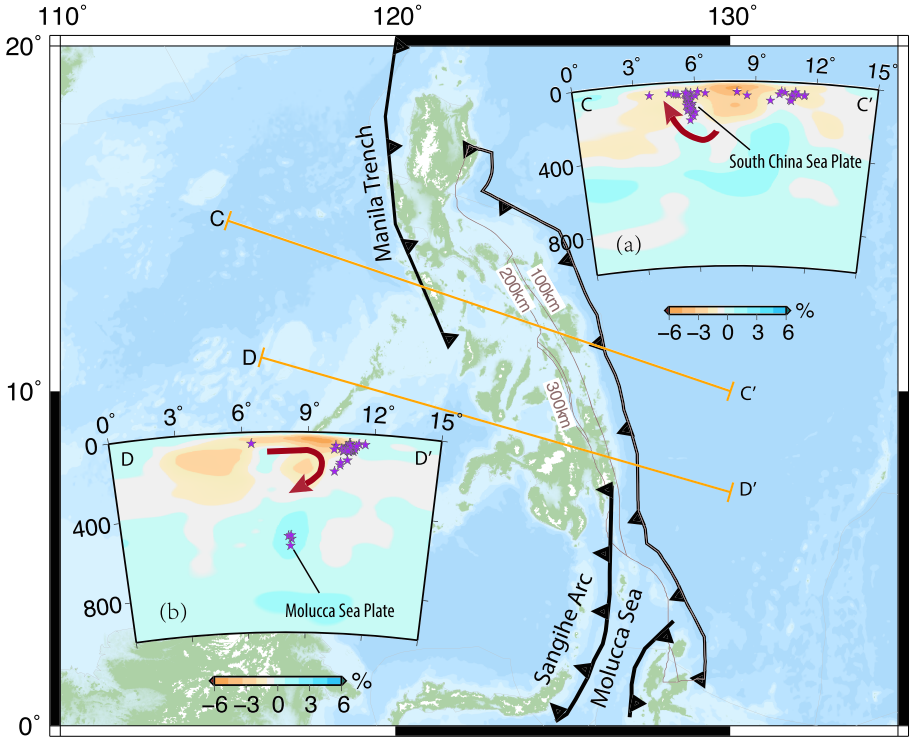

Figure 9. The same as Figure 7 but for the Philippine subduction zone. The bent arrow in the insert (a) denotes the flow associated with the edge of the eastward subducted South China Sea Plate, whereas that in the insert (b) displays the 2-D corner flow driven by the westward subduction of the Philippine Sea Plate. Notably, the isolated seismicity in the mantle transition zone (presented in the insert (b)) likely belongs to the westward subducted Molucca Sea Plate from the Sangihe trench, suggesting that the Molucca Sea Plate may play an important role in influencing the regional mantle dynamics attributable to its deep subduction.

wave splitting measurements from deep events (Di Leo et al., 2012b), which has been associated with the westward Sangihe subduction process. The trench-normal fast directions observed in this study can be readily developed by the 2-D corner flow in the mantle wedge controlled by the westward subduction of the Philippine Sea Plate, and the westward deep subduction of the Molucca Sea Plate perhaps further enhances the trench-normal flow (Zhang et al., 2017). The subduction of the Molucca Sea Plate may thus play an important role in influencing the regional mantle dynamics due to its deep subduction. By contrast, the eastward Sulu subduction may have no impact on this corner flow process due to its present subduction state characterized by lack of active seismicity and the absence of a high-velocity anomaly beneath the Sulu Sea (Hall & Spakman, 2015). To the north, the fast directions from our observations become more diverse, and trench oblique is evident. This scattered phenomenon is likely caused by the interaction between the westward Philippine Sea Plate and eastward South China Sea Plate, whereas the trench-parallel fast directions may be a result of the edge effect; the mantle flow has long been recognized to be deflected due to close proximity to the edges of subducting slabs. Such a toroidal flow around lateral slab edges has been suggested in both numerical simulations (e.g., Honda, 2009; Jadamec & Billen, 2010; Kneller & van Keken, 2008) and analog models (e.g., Buttles & Olson, 1998; Schellart, 2004).

In order to better understand the dynamic processes, the tomographic model UU-P07 of Hall and Spakman (2015) is also employed in this area to help with interpretations (Figure 9). Figure 9 clearly shows that the 2-D corner flow associated with slow anomaly of asthenospheric materials can be readily developed by the westward subduction of the Philippine Sea Plate; it also demonstrates that a cluster of earthquakes is located in the mantle transition zone, which likely belong to the stagnant slab of the westward subducted Molucca Sea Plate from the Sangihe trench (Zhang et al., 2017). The deep Sangihe subduction may thus play a role in influencing the regional dynamics. By contrast, to the north, there is no deep subduction as suggested from the seismicity distribution along the downgoing slabs (Figure 9b). As a result, the 2-D corner flow may not be well developed, but the low-velocity anomalies in the upper mantle located in between

the South China Sea Plate and Philippine Sea Plate are clearly imaged by the tomography result. We thus envisage that a lateral flow could also be developed by squeezing the asthenospheric materials between the two oppositely dipping and adjacent subducting slabs. It is notable that the trench-parallel fast direction in this area (Figures 5 and 6) is evident by the surface wave tomographic result (Debayle et al., 2016), which appears to favor this hypothesis. This envisaged scenario certainly needs to be verified by more investigations in the future. Moreover, as we suggested above, we attribute the trench-parallel flow to the edge effect by the eastward subducted South China Sea Plate. It is possible that the flow is wrapping around the slab edge as suggested to occur in other subduction zones like in Alaska (e.g., Venereau et al., 2019) and Ryukyu (Kuo et al., 2012) but which needs more observations to draw a conclusion. The interpreted 2-D corner flow and deflected flow due to edge effect in this area are both displayed schematically in Figure 8. Our observations thus demonstrate that slab-slab interactions actively occur in the complex tectonic region.

6.3. Mantle Flow Systems Beneath the Sunda Plate

Several different flow features beneath the Sunda Plate have been inferred. According to our observations, simple 2-D corner flow induced by viscous coupling between the downgoing slab and overlying mantle is observed in both the Java and Philippine subduction zones; it will certainly play a dominant role in making up the flow systems beneath the Sunda Plate. The lateral flow developed by highly arcuate subducting slab in Banda and trench-oblique flow caused by the eastward subduction of the South China Sea Plate in Philippines will additionally contribute to the flow systems. Moreover, other flows with different geometry will certainly serve as important components in the flow systems, including nearly trench-normal-oriented flow (Figure 6) (more likely a 2-D corner flow) induced by the eastward subduction of the Indo-Burman plate observed beneath the southern Indochina Peninsula (Yu et al., 2018); a 3-D toroidal flow around lateral slab edges of the Celebes Sea slab suggested by Di Leo et al. (2012a); and a 3-D toroidal flow in the Sumatra mantle wedge associated with slab tear observed by Huang et al. (2015). The subslab mantle flow around the highly arcuate Banda slab, if it exists, may also contribute to the flow systems beneath the Sunda Plate. A future study on the subslab anisotropy below the subducting Philippine Sea Plate and South China Sea Plate is also necessary to understand how the subslab mantle flow will influence the mantle flow systems beneath the Sunda Plate.

In addition, the flow geometry beneath the South China Sea has barely been investigated, in particular that associated with the Hainan mantle plume (e.g., Liu et al., 2018; Mériaux et al., 2015; Yu et al., 2018), which has not been detected. A future investigation of mantle flow beneath the South China Sea is thus important to understand how the Hainan plume has been influencing the flow systems beneath the Sunda Plate.

Figure S5 illustrates the main conclusions from our study. It shows the dynamic processes driving seismic anisotropy at the Banda-Java subduction zone and the central to north Philippine subduction zone, in which a slab tear is suggested to exist in the downgoing Indian Plate beneath the Sumatra-Java border (Huang et al., 2015; Srijayanthi & Kumar, 2019) and a subslab flow around the highly arcuate Banda slab driven by slab rollback is suggested by Di Leo et al. (2012a). Therefore, the flow systems beneath the Sunda Plate appear to be primarily controlled by its surrounding subduction plates.

7. Summary

We have performed a source-side *sS* splitting study of backarc regions in the Java-Banda and Philippine subduction zones, and our results present new constrains on the mantle dynamics in the study area. A total of 37 measurements is obtained. Overall, the delay times vary from 0.4 to 2.0 s with an average of 0.96 s and a standard deviation of 0.36 s. The fast directions abundantly exhibit either trench normal or trench parallel. For both the subduction zones, the trench-normal fast directions in mantle wedge could be developed by 2-D corner flow. A fast direction rotation from trench normal to trench parallel is observed in the Java-Banda subduction zone, which is a result of interactions between a 2-D corner flow and a squeezed asthenospheric flow by the highly arcuate Banda slab, whereas the trench-oblique signature is observed in the north Philippine subduction zone, which may be deflected due to the eastward subduction of the South China Sea Plate. The flow system beneath the Sunda plate may thus be a result of the interactions of different types of flow in the subduction zones. The resultant flow system may have an influence on the mantle dynamics under the adjacent South China Sea. More importantly, our observations will complement the global compilation of mantle wedge anisotropy in subduction zones by Long and Wirth (2013).

Acknowledgments
The manuscript benefits from constructive reviews by Yi Cao and David Yuen. We are grateful to the thoughtful and constructive comments provided by three anonymous reviewers and the editor, which helped to improve the manuscript considerably. The waveform data from the networks (SD, SN, QH, and NX) are downloaded from the seismic data center in China (http://www.seisdmc.ac.cn), whereas the seismic data from the networks (KN, KR, II, G, AK, KZ, and IU) are downloaded from the Data Management Center of the Incorporated Research Institutions for Seismology (www.iris.edu). All the 37 *sS* waveforms in the horizontal components used in this study can be accessed from http://doi.org/10.5281/zenodo.3366111. Some figures were prepared using Generic Mapping Tools (Wessel & Smith, 1991) and GNUPLOT. This work was funded by the National Science Foundation of China (Grants 91428309 and 41761134051).

References

Abers, G. A. (2000). Hydrated subducted crust at 100–250 km depth. *Earth and Planetary Science Letters*, *176*(3), 323–330.

Anglin, D. K., & Fouch, M. J. (2005). Seismic anisotropy in the Izu-Bonin subduction system. *Geophysical Research Letters*, *32*, L09307. https://doi.org/10.1029/2005GL022714

Audet, P. (2013). Seismic anisotropy of subducting oceanic uppermost mantle from fossil spreading. *Geophysical Research Letters*, *40*, 173–177. https://doi.org/10.1029/2012GL054328

Baccheschi, P., Margheriti, L., Steckler, M. S., & Boschi, E. (2011). Anisotropy patterns in the subducting lithosphere and in the mantle wedge: A case study—The southern Italy subduction system. *Journal of Geophysical Research*, *116*, Q05S15. https://doi.org/10.1029/2010JB007961

Barruol, G., & Ben Ismail, W. (2001). Upper mantle anisotropy beneath the African IRIS and Geoscope stations. *Geophysical Journal International*, *146*, 549–561. https://doi.org/10.1046/j.0956-540x.2001.01481.x

Barruol, G., & Hoffman, R. (1999). Upper mantle anisotropy beneath the Geoscope stations. *Journal of Geophysical Research*, *104*(B5), 10,757–10,773. https://doi.org/10.1029/1999JB900033

Bird, P. (2003). An updated digital model of plate boundaries. *Geochemistry, Geophysics, Geosystems*, *4*(3), 1027. https://doi.org/10.1029/2001GC000252

Bodmer, M., Toomey, D. R., Hooft, E. E., Nábelek, J., & Braunmiller, J. (2015). Seismic anisotropy beneath the Juan de Fuca plate system: Evidence for heterogeneous mantle flow. *Geology*, *43*(12), 1095–1098. https://doi.org/10.1130/G37181.1

Bowman, J. R., & Ando, M. (1987). Shear-wave splitting in the upper-mantle wedge above the Tonga subduction zone. *Geophysical Journal International*, *88*(1), 25–41. https://doi.org/10.1111/j.1365-246X.1987.tb01367.x

Buttles, J., & Olson, P. (1998). A laboratory model of subduction zone anisotropy. *Earth and Planetary Science Letters*, *164*(1-2), 245–262.

Chang, S.-J., & Ferreira, A. M. G. (2019). Inference on water content in the mantle transition zone near subducted slabs from anisotropy tomography. *Geochemistry, Geophysics, Geosystems*, *20*, 1189–1201. https://doi.org/10.1029/2018GC008090

Chang, L., Flesch, L. M., Wang, C.-Y., & Ding, Z. (2015). Vertical coherence of deformation in lithosphere in the eastern Himalayan syntaxis using GPS, Quaternary fault slip rates, and shear wave splitting data. *Geophysical Research Letters*, *42*, 5813–5819. https://doi.org/10.1002/2015GL064568

Chang, L., Wang, C., & Ding, Z. (2011). Upper mantle anisotropy in the Ordos Block and its margins. *Science China Earth Sciences*, *54*(6), 888–900.

Chen, K. H., Tseng, Y.-L., Furumura, T., & Kennett, B. L. N. (2015). Anisotropy in the subducting slab: Observations from Philippine Sea Plate events in Taiwan. *Geophysical Research Letters*, *42*, 10,248–10,255. https://doi.org/10.1002/2015GL066227

Cherie, S. G., Gao, S. S., Liu, K. H., Elsheikh, A. A., Kong, F., Reed, C. A., & Yang, B. B. (2016). Shear wave splitting analyses in Tian Shan: Geodynamic implications of complex seismic anisotropy. *Geochemistry, Geophysics, Geosystems*, *17*, 1975–1989. https://doi.org/10.1002/2016GC006269

Christensen, N. I. (1984). The magnitude, symmetry and origin of upper mantle anisotropy based on fabric analyses of ultramafic tectonites. *Geophysical Journal International*, *76*(1), 89–111. https://doi.org/10.1111/j.1365-246X.1984.tb05025.x

Collings, R., Rietbrock, A., Lange, D., Tilmann, F., Nippress, S., & Natawidjaja, D. (2013). Seismic anisotropy in the Sumatra subduction zone. *Journal of Geophysical Research: Solid Earth*, *118*, 5372–5390. https://doi.org/10.1002/jgrb.50157

Crotwell, H. P., Owens, T. J., & Ritsema, J. (1999). The TauP Toolkit: Flexible seismic travel-time and ray-path utilities. *Seismological Research Letters*, *70*(2), 154–160. https://doi.org/10.1785/gssrl.70.2.154

DeMets, C., Gordon, R. G., Argus, D. F., & Stein, S. (1994). Effect of recent revisions to the geomagnetic reversal time scale on estimates of current plate motions. *Geophysical Research Letters*, *21*(20), 2191–2194. https://doi.org/10.1029/94GL02118

Debayle, E., Dubuffet, F., & Durand, S. (2016). An automatically updated S-wave model of the upper mantle and the depth extent of azimuthal anisotropy. *Geophysical Research Letters*, *43*, 674–682. https://doi.org/10.1002/2015GL067329

Debayle, E., & Ricard, Y. (2013). Seismic observations of large-scale deformation at the bottom of fast-moving plates. *Earth and Planetary Science Letters*, *376*(C), 165–177. https://doi.org/10.1016/j.epsl.2013.06.025

Di Leo, J. F., Wookey, J., Hammond, J. O. S., Kendall, J. M., Kaneshima, S., Inoue, H., et al. (2012a). Mantle flow in regions of complex tectonics: Insights from Indonesia. *Geochemistry, Geophysics, Geosystems*, *13*, Q12008. https://doi.org/10.1029/2012GC004417

Di Leo, J. F., Wookey, J., Hammond, J. O. S., Kendall, J. M., Kaneshima, S., Inoue, H., et al. (2012b). Deformation and mantle flow beneath the Sangihe subduction zone from seismic anisotropy. *Physics of the Earth and Planetary Interiors*, *194-195*(C), 38–54. https://doi.org/10.1016/j.pepi.2012.01.008

Eakin, C. M., Obrebski, M., Allen, R. M., Boyarko, D. C., Brudzinski, M. R., & Porritt, R. (2010). Seismic anisotropy beneath Cascadia and the Mendocino triple junction: Interaction of the subducting slab with mantle flow. *Earth and Planetary Science Letters*, *297*(3-4), 627–632. https://doi.org/10.1016/j.epsl.2010.07.015

Faccenda, M. (2014). Mid mantle seismic anisotropy around subduction zones. *Physics of the Earth and Planetary Interiors*, *227*(C), 1–19. https://doi.org/10.1016/j.pepi.2013.11.015

Faccenda, M., Burlini, L., Gerya, T. V., & Mainprice, D. (2008). Fault-induced seismic anisotropy by hydration in subducting oceanic plates. *Nature*, *455*(7216), 1097–1100. https://doi.org/10.1038/nature07376

Faccenda, M., Ferreira, A. M. G., Tisato, N., Lithgow-Bertelloni, C., Stixrude, L., & Pennacchioni, G. (2019). Extrinsic elastic anisotropy in a compositionally heterogeneous Earth's mantle. *Journal of Geophysical Research: Solid Earth*, *211*, 1585. https://doi.org/10.1029/2018JB016482

Faccenna, C., & Becker, T. W. (2010). Shaping mobile belts by small-scale convection. *Nature*, *465*(7298), 602–605. https://doi.org/10.1038/nature09064

Farra, V., & Vinnik, L. (1994). Shear-wave splitting in the mantle of the Pacific. *Geophysical Journal International*, *119*(1), 195–218. https://doi.org/10.1111/j.1365-246X.1994.tb00922.x

Ferreira, A. M. G., Faccenda, M., Sturgeon, W., Chang, S.-J., & Schardong, L. (2019). Ubiquitous lower-mantle anisotropy beneath subduction zones. *Nature Geoscience*, *12*, 301–306. https://doi.org/10.1038/s41561-019-0325-7

Fischer, K. M., & Yang, X. (1994). Anisotropy in Kuril-Kamchatka subduction zone structure. *Geophysical Research Letters*, *21*(1), 5–8. https://doi.org/10.1029/93GL03161

Fouch, M. J., & Fischer, K. M. (1996). Mantle anisotropy beneath northwest Pacific subduction zones. *Journal of Geophysical Research*, *101*(B7), 15,987–16,002. https://doi.org/10.1029/96JB00881

Fouch, M. J., & Rondenay, S. (2006). Seismic anisotropy beneath stable continental interiors. *Physics of the Earth and Planetary Interiors*, *158*(2-4), 292–320. https://doi.org/10.1016/j.pepi.2006.03.024

Gaherty, J. B., Lizarralde, D., Collins, J. A., Hirth, G., & Kim, S. (2004). Mantle deformation during slow seafloor spreading constrained by observations of seismic anisotropy in the western Atlantic. *Earth and Planetary Science Letters*, *228*(3-4), 255–265. https://doi.org/10.1016/j.epsl.2004.10.026

Gripp, A. E., & Gordon, R. G. (2002). Young tracks of hotspots and current plate velocities. *Geophysical Journal International*, *150*(2), 321–361. https://doi.org/10.1046/j.1365-246X.2002.01627.x

Hall, R., & Spakman, W. (2015). Mantle structure and tectonic history of SE Asia. *Tectonophysics*, *658*(C), 14–45. https://doi.org/10.1016/j.tecto.2015.07.003

Hammond, J. O. S., Wookey, J., Kaneshima, S., Inoue, H., Yamashina, T., & Harjadi, P. (2010). Systematic variation in anisotropy beneath the mantle wedge in the Java-Sumatra subduction system from shear-wave splitting. *Physics of the Earth and Planetary Interiors*, *178*(3-4), 189–201. https://doi.org/10.1016/j.pepi.2009.10.003

Hanna, J., & Long, M. D. (2012). SKS splitting beneath Alaska: Regional variability and implications for subduction processes at a slab edge. *Tectonophysics*, *530-531*, 272–285. https://doi.org/10.1016/j.tecto.2012.01.003

Hayes, G. P., Moore, G. L., Portner, D. E., Hearne, M., Flamme, H., Furtney, M., & Smoczyk, G. M. (2018). Slab2, a comprehensive subduction zone geometry model. *Science*, *88*, eaat472310. https://doi.org/10.1126/science.aat4723

He, X., & Long, M. D. (2011). Lowermost mantle anisotropy beneath the northwestern Pacific: Evidence from PcS, ScS, SKS, and SKKS phases. *Geochemistry, Geophysics, Geosystems*, *12*, Q12012. https://doi.org/10.1029/2011GC003779

He, X., Zhou, H., Ma, Y., & Niu, F. (2008). Synthetic study on SS waveform splitting and complication. *Acta Seismologica Sinica*, *21*(1), 35–45. https://doi.org/10.1007/s11589-008-0035-5

Helffrich, G., Silver, P., & Given, H. (1994). Shear-wave splitting variation over short spatial scales on continents. *Geophysical Journal International*, *119*(2), 561–573. https://doi.org/10.1111/j.1365-246X.1994.tb00142.x

Honda, S. (2009). Numerical simulations of mantle flow around slab edges. *Earth and Planetary Science Letters*, *277*(1), 112–122.

Huang, Q., Schmerr, N., Waszek, L., & Beghein, C. (2019). Constraints on seismic anisotropy in the mantle transition zone from long-period SS precursors. *Journal of Geophysical Research: Solid Earth*, *124*, 6779–6800. https://doi.org/10.1029/2019JB017307

Huang, Z., Wang, L., Zhao, D., Mi, N., & Xu, M. (2011). Seismic anisotropy and mantle dynamics beneath China. *Earth and Planetary Science Letters*, *306*(1-2), 105–117. https://doi.org/10.1016/j.epsl.2011.03.038

Huang, Z., Zhao, D., & Wang, L. (2011). Shear wave anisotropy in the crust, mantle wedge, and subducting Pacific slab under northeast Japan. *Geochemistry, Geophysics, Geosystems*, *12*, Q01002. https://doi.org/10.1029/2010GC003343

Huang, Z., Zhao, D., & Wang, L. (2015). P wave tomography and anisotropy beneath Southeast Asia: Insight into mantle dynamics. *Journal of Geophysical Research: Solid Earth*, *120*, 5154–5174. https://doi.org/10.1002/2015JB012098

Jadamec, M. A., & Billen, M. I. (2010). Reconciling surface plate motions with rapid three-dimensional mantle flow around a slab edge. *Nature*, *465*(7296), 338–341.

Jung, H., & Karato, S. i. (2001). Water-induced fabric transitions in olivine. *Science*, *293*(5534), 1460–1463. https://doi.org/10.1126/science.1062235

Kaneshima, S. (2014). Upper bounds of seismic anisotropy in the Tonga slab near deep earthquake foci and in the lower mantle. *Geophysical Journal International*, *197*(1), 351–368. https://doi.org/10.1093/gji/ggt494

Karato, S.-I., Jung, H., Katayama, I., & Skemer, P. (2008). Geodynamic significance of seismic anisotropy of the upper mantle: New insights from laboratory studies. *Annual Review of Earth and Planetary Sciences*, *36*(1), 59–95.

Katayama, I., & Karato, S.-I. (2006). Effect of temperature on the B- to C-type olivine fabric transition and implication for flow pattern in subduction zones. *Physics of the Earth and Planetary Interiors*, *157*(1-2), 33–45.

Kennett, B. L. N., & Engdahl, E. R. (1991). Traveltimes for global earthquake location and phase identification. *Geophysical Journal International*, *105*(2), 429–465. https://doi.org/10.1111/j.1365--246X.1991.tb06724.x

Király, E., Bianchi, I., & Bokelmann, G. (2012). Seismic anisotropy in the south western Pacific region from shear wave splitting. *Geophysical Research Letters*, *39*, L05302. https://doi.org/10.1029/2011GL050407

Király, Á., Capitanio, F. A., Funiciello, F., & Faccenna, C. (2016). Subduction zone interaction: Controls on arcuate belts. *Geology*, *44*(9), 715–718. https://doi.org/10.1130/G37912.1

Király, Á., Holt, A. F., Funiciello, F., Faccenna, C., & Capitanio, F. A. (2018). Modeling slab-slab interactions: Dynamics of outward dipping double-sided subduction systems. *Geochemistry, Geophysics, Geosystems*, *110*, 693–714. https://doi.org/10.1002/2017GC007199

Kneller, E. A., & van Keken, P. E. (2008). Effect of three-dimensional slab geometry on deformation in the mantle wedge: Implications for shear wave anisotropy. *Geochemistry, Geophysics, Geosystems*, *9*, Q01003. https://doi.org/10.1029/2007GC001677

Koulakov, I., Jakovlev, A., & Luehr, B. G. (2009). Anisotropic structure beneath central Java from local earthquake tomography. *Geochemistry, Geophysics, Geosystems*, *10*, Q02011. https://doi.org/10.1029/2008GC002109

Kuo, B.-Y., Wang, C. C., Lin, S.-C., Lin, C.-R., Chen, P. C., Jang, J. P., & Chang, H. K. (2012). Shear-wave splitting at the edge of the Ryukyu subduction zone. *Earth and Planetary Science Letters*, *355-356*, 262–270.

Legendre, C. P., Deffontaines, B., Bor-Shouh, H., Lee, H.-Y., & Chang, E. T. Y. (2020). Anisotropic Rayleigh-wave phase velocity maps of the Sunda Plate. *Journal of Asian Earth Sciences*, *187*, 104,094. https://doi.org/10.1016/j.jseaes.2019.104094

Lin, P.-Y. P., Gaherty, J. B., Jin, G., Collins, J. A., Lizarralde, D., Evans, R. L., & Hirth, G. (2016). High-resolution seismic constraints on flow dynamics in the oceanic asthenosphere. *Nature Publishing Group*, *535*(7613), 538–541. https://doi.org/10.1038/nature18012

Liu, H., Chen, F., Leng, W., Zhang, H., & Xu, Y. (2018). Crustal footprint of the Hainan plume beneath southeast China. *Journal of Geophysical Research: Solid Earth*, *123*, 3065–3079. https://doi.org/10.1002/2017JB014712

Liu, K. H., Gao, S. S., Gao, Y., & Wu, J. (2008). Shear wave splitting and mantle flow associated with the deflected Pacific slab beneath northeast Asia. *Journal of Geophysical Research*, *113*, B01305. https://doi.org/10.1029/2007JB005178

Long, M. D. (2009). Complex anisotropy in D" beneath the eastern Pacific from SKS-SKKS splitting discrepancies. *Earth and Planetary Science Letters*, *283*(1-4), 181–189. https://doi.org/10.1016/j.epsl.2009.04.019

Long, M. D. (2013). Constrains on subduction geodynamics from seismic anisotropy. *Reviews of Geophysics*, *51*, 76–112. https://doi.org/10.1002/rog.20008

Long, M. D., & Silver, P. G. (2008). The subduction zone flow field from seismic anisotropy: A global view. *Science*, *319*(5861), 315–318. https://doi.org/10.1126/science.1150809

Long, M. D., & Wirth, E. A. (2013). Mantle flow in subduction systems: The mantle wedge flow field and implications for wedge processes. *Journal of Geophysical Research: Solid Earth*, *118*, 583–606. https://doi.org/10.1002/jgrb.50063

Lynner, C., & Long, M. D. (2014). Sub-slab anisotropy beneath the Sumatra and circum-Pacific subduction zones from source-side shear wave splitting observations. *Geochemistry, Geophysics, Geosystems*, *15*, 2262–2281. https://doi.org/10.1002/2014GC005239

Lyu, T., Zhu, Z., & Wu, B. (2019). Subducting slab morphology and mantle transition zone upwelling in double-slab subduction models with inward-dipping directions. *Geophysical Journal International*, *218*(3), 2089–2105. https://doi.org/10.1093/gji/ggz268

Makeyeva, L. I., Vinnik, L. P., & Roecker, S. W. (1992). Shear-wave splitting and small-scale convection in the continental upper mantle. *Nature*, *358*(6382), 144–147. https://doi.org/10.1038/358144a0

Menke, W., & Levin, V. (2003). The cross-convolution method for interpreting SKS splitting observations, with application to one and two-layer anisotropic earth models. *Geophysical Journal International*, *154*(2), 379–392. https://doi.org/10.1046/j.1365-246X.2003.01937.x

Mériaux, C. A., Duarte, J. C., Schellart, W. P., & Mériaux, A. S. (2015). A two-way interaction between the Hainan plume and the Manila subduction zone. *Geophysical Research Letters*, *42*, 5796–5802. https://doi.org/10.1002/2015GL064313

Miyagi, L., Amulele, G., Otsuka, K., Du, Z., Farla, R., & Karato, S.-I. (2014). Plastic anisotropy and slip systems in ringwoodite deformed to high shear strain in the rotational Drickamer apparatus. *Physics of the Earth and Planetary Interiors*, *228*, 244–253. https://doi.org/10.1016/j.pepi.2013.09.012

Nowacki, A., Kendall, J.-M., & Wookey, J. (2012). Mantle anisotropy beneath the Earth's mid-ocean ridges. *Earth and Planetary Science Letters*, *317-318*, 1–12. https://doi.org/10.1016/j.epsl.2011.11.044

Nowacki, A., Wookey, J., & Kendall, J.-M. (2011). New advances in using seismic anisotropy, mineral physics and geodynamics to understand deformation in the lowermost mantle. *Journal of Geodynamics*, *52*(3-4), 205–228. https://doi.org/10.1016/j.jog.2011.04.003

Ohuchi, T., Fujino, K., Kawazoe, T., & Irifune, T. (2014). Crystallographic preferred orientation of wadsleyite and ringwoodite: Effects of phase transformation and water on seismic anisotropy in the mantle transition zone. *Earth and Planetary Science Letters*, *397*, 133–144. https://doi.org/10.1016/j.epsl.2014.03.066

Roy, S. K., Ravi Kumar, M., & Davuluri, S. (2017). Anisotropy in subduction zones: Insights from new source side S-wave splitting measurements from India. *Journal of Geophysical Research: Solid Earth*, *115*, 6454–6472. https://doi.org/10.1002/2017JB014314

Russo, R. M., & Silver, P. G. (1994). Trench-parallel flow beneath the Nazca plate from seismic anisotropy. *Science*, *263*(5150), 1105–1111. https://doi.org/10.1126/science.263.5150.1105

Rychert, C. A., & Shearer, P. M. (2010). Resolving crustal thickness using SS waveform stacks. *Geophysical Journal International*, *180*(3), 1128–1137. https://doi.org/10.1111/j.1365-246X.2009.04497.x

Schellart, W. P. (2004). Kinematics of subduction and subduction-induced flow in the upper mantle. *Journal of Geophysical Research*, *109*, B07401. https://doi.org/10.1029/2004JB002970

Shearer, P. M., & Orcutt, J. A. (1986). Compressional and shear wave anisotropy in the oceanic lithosphere—The Ngendei seismic refraction experiment. *Geophysical Journal International*, *87*(3), 967–1003. https://doi.org/10.1111/j.1365-246X.1986.tb01979.x

Silver, P. G. (1996). Seismic anisotropy beneath the continents: Probing the depths of geology. *Annual Review of Earth and Planetary Sciences*, *24*(1), 385–432. https://doi.org/10.1146/annurev.earth.24.1.385

Song, T.-R. A., & Kawakatsu, H. (2012). Subduction of oceanic asthenosphere: Evidence from sub-slab seismic anisotropy. *Geophysical Research Letters*, *39*, L17301. https://doi.org/10.1029/2012GL052639

Song, T.-R. A., & Kawakatsu, H. (2013). Subduction of oceanic asthenosphere: A critical appraisal in central Alaska. *Earth and Planetary Science Letters*, *367*(C), 82–94. https://doi.org/10.1016/j.epsl.2013.02.010

Song, T.-R. A., & Kim, Y. (2011). Anisotropic uppermost mantle in young subducted slab underplating Central Mexico. *Nature Geoscience*, *5*(1), 55–59. https://doi.org/10.1038/ngeo1342

Spakman, W., & Hall, R. (2010). Surface deformation and slab-mantle interaction during Banda arc subduction rollback. *Nature Geoscience*, *3*(8), 562–566. https://doi.org/10.1038/ngeo917

Srijayanthi, G., & Kumar, M. R. (2019). Subslab anisotropy in the Andaman subduction zone controlled by slab dip?. *Physics of the Earth and Planetary Interiors*, *286*, 21–28. https://doi.org/10.1016/j.pepi.2018.10.010

Venereau, C. M. A., Martin Short, R., Bastow, I. D., Allen, R. M., & Kounoudis, R. (2019). The role of variable slab dip in driving mantle flow at the eastern edge of the Alaskan subduction margin: Insights from shear-wave splitting. *Geochemistry, Geophysics, Geosystems*, *20*, 2433–2448. https://doi.org/10.1029/2018GC008170

Vinnik, L. P., & Farra, V. (1992). Multiple-SCS technique for measuring anisotropy in the mantle. *Geophysical Research Letters*, *19*(5), 489–492. https://doi.org/10.1029/92gl00196

Vinnik, L. P., Makeyeva, L. I., Milev, A., & Usenko, A. Y. (1992). Global patterns of azimuthal anisotropy and deformations in the continental mantle. *Geophysical Journal International*, *111*(3), 433–447. https://doi.org/10.1111/j.1365-246X.1992.tb02102.x

Walpole, J., Wookey, J., Kendall, J.-M., & Masters, T.-G. (2017). Seismic anisotropy and mantle flow below subducting slabs. *Earth and Planetary Science Letters*, *465*, 155–167. https://doi.org/10.1016/j.epsl.2017.02.023

Wessel, P., & Smith, W. H. F. (1991). Free software helps map and display data. *EOS, Transactions American Geophysical Union*, *72*(41), 441–441. https://doi.org/10.1029/90EO00319

Wolfe, C. J., & Silver, P. G. (1998). Seismic anisotropy of oceanic upper mantle: Shear wave splitting methodologies and observations. *Journal of Geophysical Research*, *103*(1), 749–771. https://doi.org/10.1029/97JB02023

Wolfe, C. J., & Solomon, S. (1998). Shear-wave splitting and implications for mantle flow beneath the MELT region of the east Pacific rise. *Science*, *280*(5367), 1230–1232. https://doi.org/10.1126/science.280.5367.1230

Wolfe, C. J., & Vernon III, F. L. (1998). Shear-wave splitting at central Tien Shan: Evidence for rapid variation of anisotropic patterns. *Geophysical Research Letters*, *25*(8), 1217–1220. https://doi.org/10.1029/98GL00838

Wookey, J., Kendall, J.-M., & Barruol, G. (2002). Mid-mantle deformation inferred from seismic anisotropy. *Nature*, *415*(6873), 777–780. https://doi.org/10.1038/415777a

Wustefeld, A., Bokelmann, G., Zaroli, C., & Barruol, G. (2008). SplitLab: A shear-wave splitting environment in MATLAB. *Computers and Geosciences*, *34*(5), 515–528. https://doi.org/10.1016/j.cageo.2007.08.002

Xue, M., Le, K. P., & yang, t. (2013). Seismic anisotropy surrounding South China Sea and its geodynamic implications. *Marine Geophysical Researches*, *34*(3-4), 407–429. https://doi.org/10.1007/s11001-013-9194-4

Yang, X., & Fischer, K. M. (1994). Constraints on North Atlantic upper mantle anisotropy from S and SS phases. *Geophysical Research Letters*, *21*(4), 309–312. https://doi.org/10.1029/93gl03261

Yu, Y., Gao, S. S., Liu, K. H., Yang, T., Xue, M., Le, K. P., & Gao, J. (2018). Characteristics of the mantle flow system beneath the Indochina Peninsula revealed by teleseismic shear wave splitting analysis. *Geochemistry, Geophysics, Geosystems*, *19*, 1519–1532. https://doi.org/10.1029/2018GC007474

Yu, M., Yan, Y., Huang, C.-Y., Zhang, X., Tian, Z., Chen, W.-H., & Santosh, M. (2018). Opening of the South China Sea and upwelling of the Hainan plume. *Geophysical Research Letters*, *45*, 2600–2609. https://doi.org/10.1002/2017GL076872

Zahirovic, S., Seton, M., & Muller, R. D. (2014). The Cretaceous and Cenozoic tectonic evolution of Southeast Asia. *Solid Earth*, *5*(1), 227–273. https://doi.org/10.5194/se-5-227-2014

Zhang, Q., Guo, F., Zhao, L., & Wu, Y. (2017). Geodynamics of divergent double subduction: 3-D numerical modeling of a Cenozoic example in the Molucca Sea region, Indonesia. *Journal of Geophysical Research: Solid Earth*, *122*, 3977–3998. https://doi.org/10.1002/2017JB013991

Zhang, S., & Karato, S.-I. (1995). Lattice preferred orientation of olivine aggregates deformed in simple shear. *Nature*, *375*(6534), 774–777. https://doi.org/10.1038/375774a0